

Enhanced Operational Stability by Cavity Control of Single-Layer Organic Light-Emitting Diodes Based on Thermally Activated Delayed Fluorescence

Yungui Li,* Bas Van der Zee, Xiao Tan, Xin Zhou, Gert-Jan A. H. Wetzelaer, and Paul W. M. Blom

Highly efficient organic light-emitting diodes (OLEDs) based on thermally activated delayed fluorescence (TADF) emitters are realized in recent years, but the device lifetime needs further improvement for practical display or lighting applications. In this work, a device design principle is presented by tuning the optical cavity of single-layer undoped devices, to realize efficient and long-lived TADF OLEDs. Extending the cavity length to the second-order interference maximum by increasing the emissive layer thickness broadens the recombination zone, while the optical outcoupling efficiency remains close to that of the thinner first-order devices. Such a device design leads to efficient and stable single-layer undoped OLEDs with a maximum external quantum efficiency of 16%, an LT_{90} of 452 h, and an LT_{50} of 3693 h at an initial luminance of 1000 cd m^{-2} , which is doubled compared to the first-order counterparts. It is further demonstrated that the widely-used empirical relation between OLED lifetime and light intensity originates from triplet–polaron annihilation, resulting in an extrapolated LT_{50} at 100 cd m^{-2} of close to 90 000 h, approaching the demands for practical backlight applications.

splitting (ΔE_{ST}) is comparable to the thermal energy.^[3] A multiple-layer structure is normally needed to balance charge carrier transport, confine charges, and excitons within the emissive layer, and place the emission zone at the optimal position inside the optical microcavity.^[2] Highly efficient monochromic TADF OLEDs have been realized by material design and device structure engineering, with the maximum external quantum efficiency (EQE) close to 40%.^[4,5] The next step is simultaneously achieving a long operational lifetime and high-efficiency TADF OLEDs for practical applications.^[6–12]


We have recently demonstrated efficient and stable OLEDs based on a single layer of the undoped TADF emitter CzDBA (9,10-bis(4-(9H-carbazol-9-yl)-2,6-dimethylphenyl)-9,10-diboraanthracene).^[13] Notably, the operational lifetime at an initial luminance L_0 of 1000 cd m^{-2} down to 50% of its initial value (LT_{50}) was reported to be 1880 h,

which is 19 times longer than multilayer devices with the same emitter.^[14] It has further been found that for the single-layer CzDBA OLEDs, the device degradation results from triplet–polaron annihilation (TPA).^[15] From previous research, it is clear that both the material structure and device layout configuration play important roles in operational stability.^[16–18] Using an n-type host material, Cui et al. demonstrated green TADF OLEDs with an LT_{50} of 654 h at an initial luminance of 5000 cd m^{-2} , enhancing the lifetime with a factor of ≈ 30 as compared to using p-type host material as a reference.^[19] Noda et al. showed that a slight chemical structure modification to a TADF emitter can enhance the charge transport and rISC rate, contributing to improved device performance and operational stability.^[20] In addition, different device design strategies have been introduced to enhance the device's lifetime. Zhang et al. demonstrated that a gradient doping concentration in the recombination zone can enhance the lifetime of a blue phosphorescent OLED by a factor of 10.^[21] Lee et al. demonstrated that the introduction of a molecular hot excited state manager can be used to receive the energy from annihilation-generated hot states before causing chemical decomposition, giving rise to a lifetime enhancement of a factor of 3.6 ± 0.1 compared to conventional, unmanaged devices.^[22]

1. Introduction

Purely organic emitters based on thermally activated delayed fluorescence (TADF) have gained tremendous attention for their use in organic light-emitting diodes (OLEDs) since there is no need for heavy atoms such as iridium or platinum to harvest triplet excitons.^[1,2] For TADF emitters, non-radiative triplets can be converted to emissive singlets via the reverse intersystem crossing (rISC) process. It is possible to obtain unity internal quantum efficiency in OLEDs when the singlet-triplet energy

Y. Li, B. Van der Zee, X. Tan, X. Zhou, G.-J. A. H. Wetzelaer, P. W. M. Blom
Max Planck Institute for Polymer Research
Ackermannweg 10, 55128 Mainz, Germany
E-mail: yungui.li@mpip-mainz.mpg.de

 The ORCID identification number(s) for the author(s) of this article can be found under <https://doi.org/10.1002/adma.202304728>

© 2023 The Authors. Advanced Materials published by Wiley-VCH GmbH. This is an open access article under the terms of the Creative Commons Attribution License, which permits use, distribution and reproduction in any medium, provided the original work is properly cited.

DOI: 10.1002/adma.202304728

Broadening the recombination zone is known to enhance the device stability, but it is also noted that it can bring side effects of device efficiency reduction.^[21] Since the cavity resonance is highly related to the emissive layer (EML) thickness, the increase of photon trapping could be one of the main reasons for quantum efficiency loss in OLEDs with a broadened recombination zone, that is, a thick EML.^[23] For application purposes, the device is normally operated under a constant luminance level, so a higher optical outcoupling efficiency can reduce the driving current density needed to reach the specific luminance. From such a perspective, the careful tuning of the optical cavity and therefore higher device efficiency is also meaningful for achieving operational stable OLEDs.

In this work, we report an OLED design strategy to maintain high device efficiency and long operation lifetime simultaneously via cavity manipulation. Extending the optical cavity length by increasing the emissive layer thickness broadens the recombination profile, leading to reduced local charge carrier and exciton density. When the optical cavity is expanded to the second-order interference maximum with the constructive resonance effect, high device efficiency can be achieved together with a long operational lifetime. Based on the TADF emitter CzDBA, we demonstrate that the second-order devices possess a maximum EQE of 16%, with an LT_{90} of 452 h at an initial luminance of 1000 cd m^{-2} . The EQE is only slightly reduced compared to the first-order device (19%), while the operational lifetime is more than doubled. We further reveal that the empirical relation between the initial luminance and the operational lifetime for TADF OLEDs originated from the TPA, indicating that the development of strategies to manipulate the exciton and polaron density is of vital importance for achieving long-lived TADF OLEDs. With such a device design, the lifetime LT_{50} at an initial luminance of 100 cd m^{-2} is close to 90 000 h, estimated by a degradation model based on the TPA process, approaching the demands for commercial applications.

2. Results and Discussion

The device design principle is schematically illustrated in **Figure 1a**. A neat CzDBA emissive layer is sandwiched between a top cathode and a bottom anode. The detailed device structure is explained in the Experimental Section. Auxiliary layers, including $\text{MoO}_3/\text{C}_{60}$ and TPBi layers, are used as interfacial layers to form Ohmic contacts for both anode and cathode.^[24] These are essentially injection layers, the OLED comprising just an emissive layer between Ohmic contacts. Electron transport, hole transport, or exciton blocking layers, as used in multilayer devices, are absent. In our device design, charge transport is fully governed by the emitter, and blocking layers are not needed owing to the charge-density profiles generated by the Ohmic contacts. When varying the emissive layer thickness, the cavity resonance is tuned correspondingly.^[25–27]

In a single-layer OLED, recombination events can occur within the entire emissive layer. The recombination profile, determined by the position-dependent Langevin-type recombination, can be calculated based on the charge-transport parameters of electrons and holes.^[28] For organic semiconductors, the charge-carrier transport has been described using the extended Gaussian disorder model (EGDM).^[29] The charge-transport parameters in the

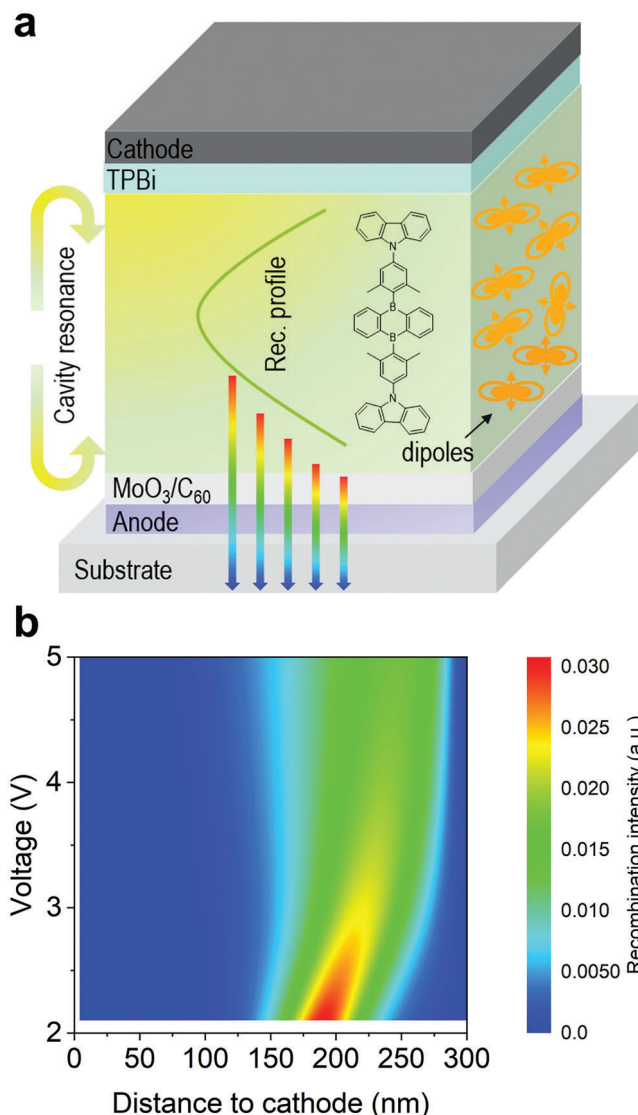


Figure 1. Device design concept. a) Schematic illustration of an OLED with a broad recombination zone based on the TADF emitter CzDBA, in which interfacial layers $\text{MoO}_3/\text{C}_{60}$ and TPBi to form Ohmic contacts for the anode and cathode have also been shown. The chemical structure is shown as an inset. b) Sum-normalized recombination profiles for a 300 nm CzDBA device, as a function of the external driving voltage, with the modeling parameters from single carrier devices fitting, as listed in Table S1 (Supporting Information).

EGDM can be obtained by fitting the temperature-dependent current density–voltage characteristics of single-carrier devices with drift-diffusion simulations.^[30] With the determined electron- and hole-transport parameters, the recombination profile for a 300 nm neat film CzDBA OLED is presented in **Figure 1b**. Since the hole mobility in CzDBA is slightly lower than the electron mobility,^[30] the peak of the recombination profile is a bit closer to the anode. When increasing the driving voltage, the recombination profile is gradually broadened, as shown in **Figure 1b**. The recombination zone at 3.0 V for CzDBA OLEDs with other different EML thicknesses is shown in **Figure 2b**. The recombination zone

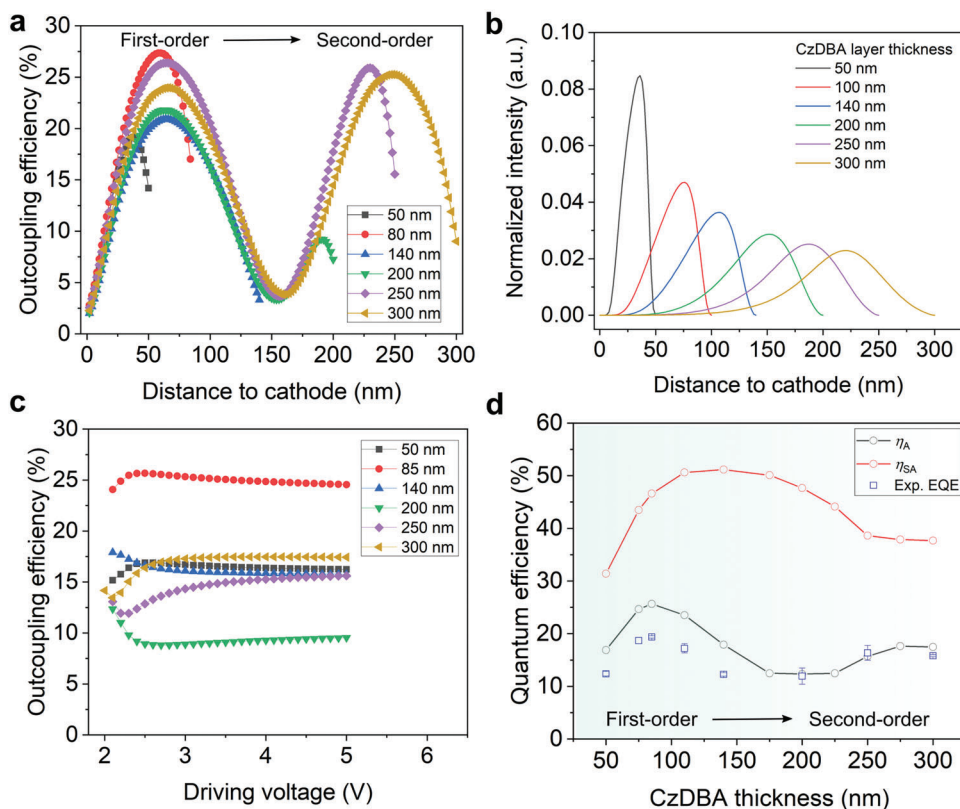


Figure 2. Optical resonance induced optical outcoupling efficiency variation. a) Position-dependent optical outcoupling to air mode for dipoles located at different positions inside the device. b) The sum-normalized recombination zone for OLEDs with different CzDBA layer thickness at 3.0 V. c) Optical outcoupling efficiency as a function of external driving voltage because of recombination zone shift. d) The maximum optical outcoupling efficiency for OLEDs with different cavity lengths. The experimental maximum EQEs from CzDBA devices are also indicated.

is gradually broadened when increasing the EML thickness since bimolecular recombination takes place within the entire EML.

For devices with a broad recombination zone, we have demonstrated that the simulation of the optical outcoupling efficiency η_{out} should be weighted by the sum-normalized recombination profile within the emissive layer,^[23] quantitatively described as:

$$\eta_{out} = \int \eta_{out}(x) \times R(x) dx \quad (1)$$

in which $\eta_{out}(x)$ is the outcoupling efficiency at the recombination position x , while $R(x)$ represents the sum-normalized recombination intensity as a function of position.

We then turn to investigate CzDBA OLEDs with different optical cavity lengths and a broad recombination zone. First, the position-dependent outcoupling efficiency η_A is simulated. The optical outcoupling efficiency to air η_A is shown in Figure 2a, the outcoupling efficiency to both substrate and air, η_{SA} , is displayed in Figure S1 (Supporting Information) for comparison. Without considering the broad recombination profile, the first-order resonance can be realized with the emitter ≈ 60 nm away from the cathode and with an entire cavity length of ≈ 80 nm. The optimized η_A in the first-order cavity is $\approx 27\%$. Further increasing the cavity length would result in destructive interference lowering the outcoupling efficiency. For example, for devices with a cavity of 200 nm, the maximum optical outcoupling is then reduced to $\approx 21\%$. Further increasing the cavity length induces the second-

order constructive interference effect. In the case of devices with a 250 and 300 nm emissive layer thickness, two emitter positions with optimized outcoupling efficiency have been resolved, with $\eta_A \approx 25\%$, which is close to the outcoupling efficiency for the optimized first-order cavity (Figure 2a). It is noted that the second-order maximum for the 300 nm device is slightly lower than that of 250 nm, indicating that further increasing the cavity length would again lead to destructive interference.

To calculate the total outcoupling efficiency for a single-layer device, the position-dependent outcoupling efficiency has to be weighted by the position-dependent recombination profile. As shown in Figure 1b and Figure 2b, the recombination zone is voltage and thickness dependent. Based on Equation (1), combined with the position-dependent outcoupling in Figure 2a, it is then possible to obtain the dependence of η_A and η_{SA} on external driving voltages, as shown in Figure 2c and Figure S2 (Supporting Information). The optical outcoupling efficiency varies at low voltages from 2–3 V, resulting from a slight shift in the recombination zone. The recombination profile is quite stable at higher voltages, as shown in Figure 1b.

From the voltage dependence, it is then possible to extract the maximum optical outcoupling for devices with different optical cavities, as shown in Figure 2d. The η_A is obtained considering the total emission from different positions in the entire recombination profile, so the absolute value is slightly lower compared to a device with a thin recombination zone, placed in the optimum

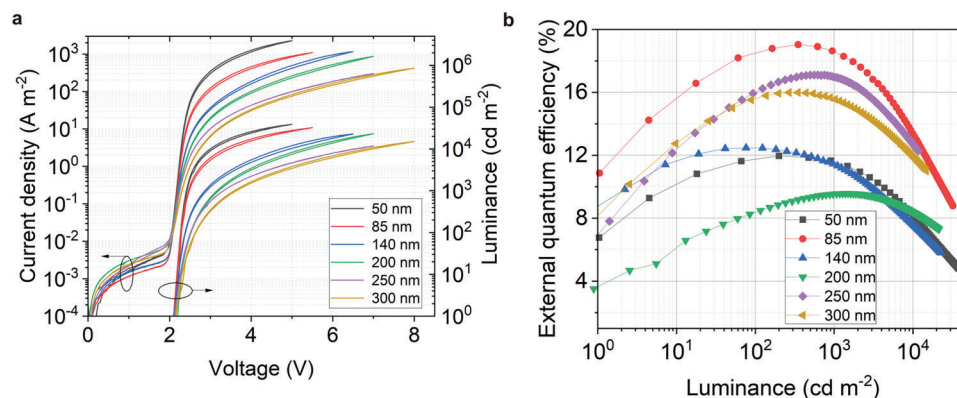


Figure 3. Device performance. a) Current density–voltage–luminance characteristics. b) Luminance-EQE.

position of the cavity. Nevertheless, the total optical outcoupling shows a similar thickness dependence when increasing the cavity length. For CzDBA OLEDs, the maximum η_A with a broad recombination zone is $\approx 25\%$ and $\approx 18\%$, for the first-order and the second-order cavity, respectively. However, it is only $\approx 12\%$ for devices with ≈ 200 nm CzDBA due to destructive interference.

The integrated optical outcoupling efficiency is slightly lower for thick devices exploiting the second-order resonance cavity. The main reason is that the broadening of the recombination zone with increasing layer thickness reduces the overlap between the emission zone and the constructive interference maxima. As a result, for thicker devices, part of the recombination events occurs at positions inside the cavity where optical outcoupling is suboptimal.

The device performance including the current density–luminance–voltage, luminance-EQE, and electroluminescence (EL) characteristics for devices with different cavity lengths is summarized in **Figure 3**. EL can be observed even at subgap voltages, with turn-on voltages as low as 2.1 V to reach 1 cd m^{-2} , resulting from the recombination of diffused and thermally generated charge carriers, which is independent of the EML thickness.^[31] A luminance of 1000 cd m^{-2} is reached at 2.5 V for the device exploiting the first-order interference maximum ($L = 85$ nm), while the voltage of 3.7 V required for the second-order device is still low.

The luminance-EQE characteristics for CzDBA OLEDs with different cavity lengths are shown in **Figure 3b**. The EQE gradually increases to its maximum at a few hundreds of cd m^{-2} , then starts to roll off because of triplet–triplet annihilation.^[32] The maximum EQE for the device with the first-order cavity ($L = 85$ nm) is $\approx 19\%$, while it is as high as 16–17% for devices with the second-order cavity ($L = 300$ nm). Thus, only a marginal EQE reduction is induced when extending the optical cavity, though the luminous efficacy has a larger decrease because of increased driving voltages, as shown in **Figure S3** (Supporting Information). The EL spectra for the second-order cavity device are shown in **Figure S4** (Supporting Information). The EL spectrum is slightly broadened at lower voltages but stable at higher bias, which may originate from a small shift of the recombination profile. The CIE color coordinate is (0.47, 0.52) at 2.5 V, which is close to one of the first-order cavity devices.^[13]

The operational lifetimes of the OLEDs are summarized in **Figure 4**. As shown in **Figure 4a**, the operational stability is gradually increased when increasing the cavity length. The LT_{90} at an L_0 of 1000 cd m^{-2} for CzDBA devices with different optical cavity lengths are shown in **Figure 4b** and **Figures S5–S7** (Supporting Information). We note that in **Figure 4b** also the previously reported lifetime for OLEDs with 75 nm CzDBA has been included, already showing good device efficiency and long operational lifetime.^[13] The LT_{90} is only 44 h for the device with a 50 nm CzDBA layer. Tuning the cavity to the first-order maximum (85 nm) leads to a significant operational lifetime enhancement up to 231 h. Further extending the cavity length to the second-order maximum of 300 nm, the LT_{90} is enhanced to 452 h, which is ≈ 2 times longer than that of devices with the first-order cavity.

Even though extending the cavity length increases the lifetime, the increase does not seem to be linear, as displayed in **Figure 4b**. The reason is that the current efficiency is not the same for all device thicknesses due to differences in the optical outcoupling efficiencies, as shown in **Figure S3** (Supporting Information) and **Figure 2**. When stressing the devices at equal initial luminance, less efficient devices require a higher driving current density, and, as a result, the lifetime will be compromised slightly. For this example, the more efficient 140 nm device has a similar lifetime to the 200 nm device, despite the reduced cavity length.

The LT_{80} for the second-order OLEDs at different initial luminance is shown in **Figure 4c**. Typically, in the OLED community, the estimation of the lifetime at lower luminance is based on an empirical relation between the operational lifetime and the initial luminance value:^[17,19]

$$LT_{80}^{100} = LT_{80}^{Lx} \times \left(\frac{Lx}{100} \right)^n \quad (2)$$

In the above equation, LT_{80}^{Lx} is the LT_{80} for the device aged at a higher luminance Lx , while n is the degradation acceleration factor. However, a device model that incorporates a clear physical degradation mechanism that quantitatively explains the above formula is lacking. So far, justification for the degradation behavior of OLEDs has been given based on differential equations that result in a stretched exponential behavior.^[33] The acceleration factor is usually assumed to be 1.75, which how-

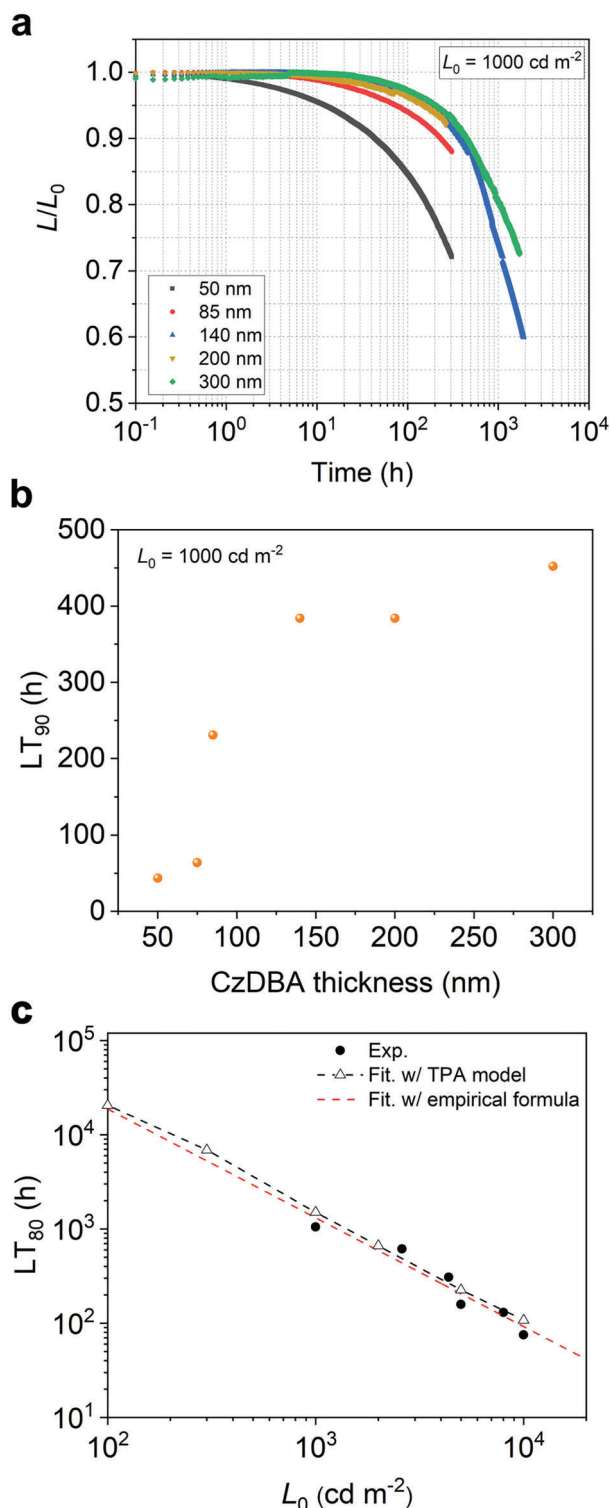


Figure 4. Cavity resonance enhanced device operational stability. a) Device degradation behavior for OLEDs with different cavity lengths. b) LT_{90} for OLEDs with L_0 at 1000 cd m^{-2} , in which the 75 nm device lifetime is extracted from a previous report as a comparison.^[113] c) LT_{80} for OLEDs with a second-order cavity with a 300 nm CzDBA layer thickness, degraded at different L_0 . The experimental degradation is compared with the empirical relation fitting and TPA degradation model prediction based on drift-diffusion device modeling.

ever may not universally apply to all OLEDs.^[33] The LT_{80} for the second-order OLEDs at different initial luminance is shown in Figure 4c, with the luminance decay measured at different initial luminance levels summarized in Figure S6 (Supporting Information). By fitting the experimental LT_{80} lifetimes with Equation (2), an acceleration factor of 1.15 is obtained, substantially lower than the acceleration factors usually assumed for phosphorescent OLEDs.^[34,35] The extrapolated LT_{80}^{100} obtained from Equation (2) equals 18 746 h.

While the obtained acceleration factor seems to be low, it should be noted that there are not that many reports about the experimental determination of the acceleration factor for TADF OLEDs. A recent study involving TADF OLEDs reported acceleration factors of 1.13 and 1.30 for a single-stack multilayer device and a double-stack tandem device, respectively.^[36] This demonstrates that small acceleration factors are not exclusive to single-layer OLEDs. Unfortunately, experimentally determined values like these are rather limited.

As a potential source of different acceleration factors in different OLEDs, we identify the efficiency roll-off. For devices with a strong roll-off, a comparatively higher current density is required at high luminance, implying faster degradation. Some experimental observations can support this deduction. A 140 nm CzDBA OLED has a slightly higher acceleration factor than a 300 nm device, and also exhibits stronger efficiency roll-off, as shown in Figures S7 and S8 (Supporting Information). As a result, the dependence of the driving current on luminance is also slightly stronger for the 140 nm device, considering the similar optical outcoupling efficiency for these two devices. However, as these are the same types of OLEDs, the difference is very minor.

The simplicity of the structure of single-layer CzDBA OLEDs allows us to quantitatively address device degradation using a numerical device model. In order to explain the physical origin of the dependence of the lifetime on initial luminance, we recall that the degradation in CzDBA OLEDs mainly results from the generation of charge carrier traps by TPA, in which the trap generation rates are correlated to the product of the charge-carrier and triplet densities.^[15] In this model, the lifetime is described with drift-diffusion simulations, which contain the experimental charge-transport parameters and the resulting positional dependence of the charge and exciton densities. The model consistently describes the voltage increase when aging at a constant current with a proportionality constant for the trap formation rate as only an unknown input parameter. Knowing this constant then allows us to predict the dependence of OLED lifetime as a function of light intensity, which has been previously determined from the voltage increase and luminance decay under current stress.^[15] As such, this model does not contain any fitting parameters to describe the dependence of the lifetime on the initial luminance. Therefore, we also use the TPA model to describe the LT_{80} for the 300 nm CzDBA OLEDs under different initial luminance levels, that is, charge carrier and exciton densities. As shown in Figure 4c, the experimental and TPA-modelled result agrees very well, with the TPA-modelled LT_{80}^{100} of 20 510 h. Remarkably, the predicted trend of OLED lifetime with light intensity also closely follows the fit from the empirical model over 2 orders of magnitude. This shows that a device model using TPA as the main degradation mechanism can fully reproduce the trend of the widely-used empirical relation.

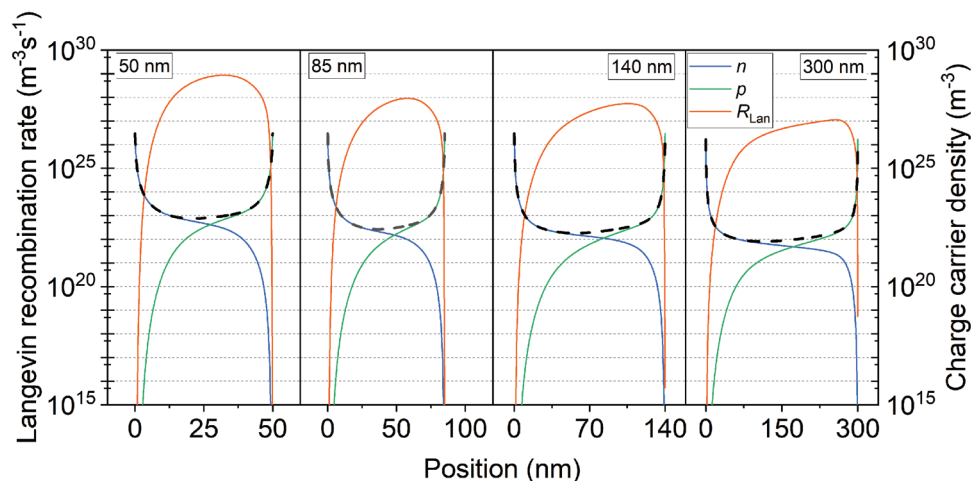


Figure 5. Mechanism of cavity tuning enhanced device stability. Position-dependent electron- (n) and hole (p) densities at the given current densities to obtain 1000 cd m^{-2} are presented. The black dashed line is the sum of the electron and hole densities. The Langevin recombination rate R_{Lan} to form excitons is plotted to demonstrate the difference in exciton density.

For backlight purposes, the luminance level required can be down to 100 cd m^{-2} . Considering the good match between the LT_{80} s estimated by the physically defined TPA model and the experimentally measured values at different initial luminance levels, we apply the same TPA model to estimate the LT_{50}^{100} , which is as long as 89 423 h, as shown in Figure S9 (Supporting Information). Notably, it is among the most long-lived single-unit (non-tandem) yellow TADF OLEDs. Representative yellow TADF OLEDs with their maximum EQE, emissive color, and lifetime values at the initial luminance of 1000 cd m^{-2} are summarized in Table S2 (Supporting Information), though some of the reported lifetimes were obtained by fitting with Equation (2) with an acceleration factor as large as 1.7–1.75.^[11,13,37–39] It should be noted that the estimated LT_{50}^{100} for 300 nm CzDBA OLEDs in this work would be more than 660 000 h, with an acceleration factor of 1.75 based on the experimentally measured LT_{50} (209.2 h) at the initial luminance of $10\,000 \text{ cd m}^{-2}$, as shown in Figure S6 (Supporting Information).

To obtain more insight into the effect of cavity thickness on the device lifetime, the charge carrier densities to achieve 1000 cd m^{-2} are plotted in Figure 5, while the Langevin recombination rate is shown to visualize the significant difference in exciton density when extending the cavity length. Since the charge carrier transport is quite balanced for CzDBA OLEDs, the peak of the recombination profile is not far from the center of the emissive layer (Figure 1b). Therefore, we can compare the densities in the middle of the neat film to estimate the role of annihilation processes for CzDBA OLEDs with different cavities. The corresponding electron density is $\approx 4.7 \times 10^{22} \text{ m}^{-3}$ for the 50 nm CzDBA OLED, being reduced to $1.8 \times 10^{22} \text{ m}^{-3}$ for the 85 nm device, a reduction by a factor of 2.5. Similarly, the exciton density is found to be reduced by a factor of 12. Such a density decrease strongly reduces the polaron–exciton annihilation, which is responsible for the degradation. Therefore, the LT_{90} at 1000 cd m^{-2} of the 85 nm OLEDs (230 h) is higher (5.3 times) than that of the 50 nm OLEDs (20.3 h). Extending the optical cavity to the second-order outcouple maximum with a CzDBA thickness of 300 nm, the electron density is decreased further to $5.4 \times 10^{21} \text{ m}^{-3}$, while

the exciton density is reduced by another factor of 10, compared to the first-order device (85 nm). Therefore, material decomposition induced by TPA is suppressed even further, giving rise to an increase of LT_{90} to 452 h, with a factor of 2 compared to 85 nm CzDBA devices with the first-order constructive interference resonance. Because the outcoupling efficiency is close for the first-order and the second-order devices, the lifetime change is mainly resulting from the impact of recombination zone expansion on the device's electrical properties. The high optical outcoupling efficiency is thus another positive effect obtained by extending the resonance cavity to the second-order interference maximum, which in the end leads to high EQE.

Such a device design principle can be used for other TADF emitters with balanced charge transport, in which the recombination zone can be tuned by the layer thickness. For emitters with significant trapping or unbalanced transport which can be experimentally verified by single-carrier devices,^[40–42] the recombination zone is less sensitive toward the change of the emissive layer thickness, with the recombination profile mainly located in the vicinity of electrode interface injecting the charge carrier with lower effective mobility.^[43,44]

To explore the potential of exploiting the second-order cavity for single-layer OLEDs of different colors, we carried out additional simulations for different emission spectra. When assuming the emitters in the blue and green OLEDs with photoluminescence spectra in Figure S10a (Supporting Information), we can then estimate the optical effect of broadening the emissive layer thickness, with an assumed dipole orientation factor in a reasonable range. Here, for simplicity, the dipole orientation factor is assumed to be 0.148 (same as for CzDBA), with the same device structure shown in Figure 1a. The optical constants and photoluminescence spectra are the experimental values obtained for the blue emitter 10,10'-(4,4'-Sulfonylbis(4,1-phenylene))bis(9,9-dimethyl-9,10-dihydroacridine) (DMAC-DPS) and the green emitter bis[4-(9,9-dimethyl-9,10-dihydroacridine)phenyl]methanone (DMAC-BP). The position of both the first- and second-order constructive interference maxima shift slightly toward shorter distances from

the metallic cathode and have their maximum value for shorter cavity lengths (Figure S10b,c, Supporting Information), as expected. The maximum values are dependent on the exact optical parameters chosen, which differ for different materials. Assuming the same charge-transport parameters as for CzDBA, the integrated optical outcoupling efficiency (Figure S10d, Supporting Information) shows a similar trend for green and blue OLEDs, but with slightly reduced optimal cavity lengths because of the shorter wavelength emission. It is demonstrated that also for green and blue OLEDs a similar difference in outcoupling efficiency can be expected when moving from the first-order to the second-order cavity. These simulation results demonstrate that a similar effect can be maintained for blue and green OLEDs, based on emitters that have shown excellent device performance in host materials or neat films if balanced charge transport is maintained.^[45–48] Therefore, broadening the recombination zone to the second-order cavity resonance maximum has general importance for achieving efficient and stable OLEDs, regardless of the emissive color.

It is worth noting that the strategy presented here is fundamentally different from exploiting the second-order cavity in multilayer OLEDs. In multilayer OLEDs, this is achieved by tuning the thickness of the doped charge transport layer, rather than the thickness of the emissive layer as reported in the present work.^[26,27] Since the emission zone is not broadened, triplet–polaron interactions remain similar in such devices. In the present work, the device is designed in a single-layer manner, without the need for the charge transport layer. Extending the optical cavity reduces triplet–polaron interactions, leading to a long operational lifetime, while maintaining high device efficiency because of constructive optical interference.

3. Conclusion

In summary, we presented a device design strategy to simultaneously obtain high efficiency and long operational lifetime for OLEDs based on TADF emitters by extending the optical cavity of single-layer OLEDs. Using OLEDs with a neat CzDBA film as the emissive layer, expanding the optical cavity to the second-order constructive interference maximum and thereby broadening the recombination zone can improve the operational lifetime by a factor of 2 while maintaining a high external quantum efficiency of $\approx 16\%$. In the end, the second-order devices possess an LT_{90} lifetime of 452 h at an initial luminance of 1000 cd m^{-2} . Based on a physically meaningful TPA degradation model, the estimated LT_{50} at 100 cd m^{-2} is close to 90 000 h, reaching a level that becomes interesting for applications. We anticipate that the work can open avenues for highly efficient and operationally stable single-layer TADF OLEDs, which accelerates their utilization in display and lighting products.

4. Experimental Section

OLED Fabrication: ITO substrates were cleaned with detergent solution, before moving to an ultrasonic bath for 5 min each in acetone and isopropyl alcohol. ITO substrates were then UV-ozone treated for another 20 min. Afterward, a PEDOT: PSS (Al4083) layer (40 nm) was coated and annealed at $140 \text{ }^\circ\text{C}$. The following layers were then deposited in vacuum

chambers with a pressure of $4\text{--}6 \times 10^{-7}$ mbar. The evaporation rates and layer thicknesses were tracked by quartz crystal monitors. A layer of 6 nm MoO_3 , 3 nm C_{60} , CzDBA layer with a thickness of 50, 85, 140, 200, 250, and 300 nm were deposited, sequentially with an additional 4 nm 2,2',2''-(1,3,5-Benzinetriyl)-tris(1-phenyl-1-H-benzimidazole) (TPBi) layer. In the end, an aluminum layer ≈ 100 nm was deposited as the cathode.

Device Characterization: The voltage–current density behavior was measured with a Keithley 2400, with the light output simultaneously recorded by a calibrated Si photodiode. The calibrated Si photodiode had a larger area size to the emissive pixel and it was placed close to the OLED pixel while not touching it. The detected photons were treated as the sum of emitted photons. Integrated EL spectra were measured by a USB4000-UV–vis–ES spectrometer (Ocean optics) close to the emitting area at different driving voltages. The degradation tests were also tracked by a calibrated photodiode, with constant current densities. The maximum EQE statistics shown in Figure 2c were averaged among 5–15 devices with the standard deviation. Different current densities were set to investigate the degradation behavior with different initial luminance. These degradation measurements were done in a glove box filled with nitrogen without further encapsulation.

Recombination Profile Simulation: The voltage-dependent recombination profiles were obtained based on the EGDM.^[29] The electrical parameters were adopted from a previous systematic investigation on the transport properties of CzDBA.^[30] The parameters used in EGDM were summarized in Table S1 (Supporting Information).

Optical Simulations: The refractive index and dipole orientation factor for the CzDBA neat film was verified experimentally.^[23] For all the other materials, complex refractive indices determined by experimental measurements were used.

Supporting Information

Supporting Information is available from the Wiley Online Library or from the author.

Acknowledgements

The authors thank the technical support from Frank Keller, Christian Bauer, and the electronic workshop in Max Planck Institute for Polymer Research. Open access funding enabled and organized by Projekt DEAL.

Conflict of Interest

The authors declare no conflict of interest.

Data Availability Statement

The data that support the findings of this study are available from the corresponding author upon reasonable request.

Keywords

lifetimes, optical cavities, optical outcoupling, organic light-emitting diodes, thermally activated delayed fluorescence

Received: May 18, 2023
Revised: August 11, 2023
Published online: October 27, 2023

[1] H. Uoyama, K. Goushi, K. Shizu, H. Nomura, C. Adachi, *Nature* **2012**, 492, 234.

- [2] M. Y. Wong, E. Zysman-Colman, *Adv. Mater.* **2017**, *29*, 1605444.
- [3] F. B. Dias, K. N. Bourdakos, V. Jankus, K. C. Moss, K. T. Kamtekar, V. Bhalla, J. Santos, M. R. Bryce, A. P. Monkman, *Adv. Mater.* **2013**, *25*, 3707.
- [4] Y. X. Hu, J. Miao, T. Hua, Z. Huang, Y. Qi, Y. Zou, Y. Qiu, H. Xia, H. Liu, X. Cao, C. Yang, *Nat. Photonics* **2022**, *16*, 803.
- [5] P. Jiang, J. Miao, X. Cao, H. Xia, K. Pan, T. Hua, X. Lv, Z. Huang, Y. Zou, C. Yang, *Adv. Mater.* **2022**, *34*, 2106954.
- [6] S. K. Jeon, H. L. Lee, K. S. Yook, J. Y. Lee, *Adv. Mater.* **2019**, *31*, 1803524.
- [7] H.-G. Kim, K.-H. Kim, J.-J. Kim, *Adv. Mater.* **2017**, *29*, 1702159.
- [8] Y. Im, W. Song, J. Y. Lee, *J. Mater. Chem. C* **2015**, *3*, 8061.
- [9] R. Mac Ciarnáin, H. W. Mo, K. Nagayoshi, H. Fujimoto, K. Harada, R. Gehlhaar, T. H. Ke, P. Heremans, C. Adachi, *Adv. Mater.* **2022**, *34*, 2201409.
- [10] T. Furukawa, H. Nakanotani, M. Inoue, C. Adachi, *Sci. Rep.* **2015**, *5*, 8429.
- [11] S. Kothavale, W. J. Chung, J. Y. Lee, *J. Mater. Chem. C* **2021**, *9*, 528.
- [12] J. Park, K. J. Kim, J. Lim, T. Kim, J. Y. Lee, *Adv. Mater.* **2022**, *34*, 2108581.
- [13] N. B. Kotadiya, P. W. M. Blom, G.-J. A. H. Wetzelaer, *Nat. Photonics* **2019**, *13*, 765.
- [14] T.-L. Wu, M.-J. Huang, C.-C. Lin, P.-Y. Huang, T.-Y. Chou, R.-W. Chen-Cheng, H.-W. Lin, R.-S. Liu, C.-H. Cheng, *Nat. Photonics* **2018**, *12*, 235.
- [15] B. van der Zee, Y. Li, G.-J. A. H. Wetzelaer, P. W. M. Blom, *Phys. Rev. Appl.* **2022**, *18*, 064002.
- [16] L. S. Cui, Y. L. Deng, D. P. K. Tsang, Z. Q. Jiang, Q. Zhang, L. S. Liao, C. Adachi, *Adv. Mater.* **2016**, *28*, 7620.
- [17] D. Zhang, M. Cai, Y. Zhang, D. Zhang, L. Duan, *Mater. Horiz.* **2016**, *3*, 145.
- [18] S. Kim, H. J. Bae, S. Park, W. Kim, J. Kim, J. S. Kim, Y. Jung, S. Sul, S.-G. Ihn, C. Noh, S. Kim, Y. You, *Nat. Commun.* **2018**, *9*, 1211.
- [19] L.-S. Cui, S.-B. Ruan, F. Bencheikh, R. Nagata, L. Zhang, K. Inada, H. Nakanotani, L.-S. Liao, C. Adachi, *Nat. Commun.* **2017**, *8*, 2250.
- [20] H. Noda, H. Nakanotani, C. Adachi, *Sci. Adv.* **2018**, *4*, eaao6910.
- [21] Y. Zhang, J. Lee, S. R. Forrest, *Nat. Commun.* **2014**, *5*, 5008.
- [22] J. Lee, C. Jeong, T. Batagoda, C. Coburn, M. E. Thompson, S. R. Forrest, *Nat. Commun.* **2017**, *8*, 15566.
- [23] Y. Li, N. B. Kotadiya, B. Zee, P. W. M. Blom, G. A. H. Wetzelaer, *Adv. Opt. Mater.* **2021**, *9*, 2001812.
- [24] N. B. Kotadiya, H. Lu, A. Mondal, Y. Ie, D. Andrienko, P. W. M. Blom, G.-J. A. H. Wetzelaer, *Nat. Mater.* **2018**, *17*, 329.
- [25] M. Furno, R. Meerheim, S. Hofmann, B. Lüssem, K. Leo, *Phys. Rev. B* **2012**, *85*, 115205.
- [26] S. Hofmann, M. Thomschke, P. Freitag, M. Furno, B. Lüssem, K. Leo, *Appl. Phys. Lett.* **2010**, *97*, 253308.
- [27] R. Meerheim, M. Furno, S. Hofmann, B. Lüssem, K. Leo, *Appl. Phys. Lett.* **2010**, *97*, 253305.
- [28] L. J. A. Koster, E. C. P. Smits, V. D. Mihailetchi, P. W. M. Blom, *Phys. Rev. B* **2005**, *72*, 085205.
- [29] M. Kuik, G.-J. A. H. Wetzelaer, H. T. Nicolai, N. I. Craciun, D. M. De Leeuw, P. W. M. Blom, *Adv. Mater.* **2014**, *26*, 512.
- [30] W. Liu, N. B. Kotadiya, P. W. M. Blom, G. A. H. Wetzelaer, D. Andrienko, *Adv. Mater. Technol.* **2021**, *6*, 2000120.
- [31] Y. Li, O. Sachnik, B. Zee, K. Thakur, C. Ramanan, G. A. H. Wetzelaer, P. W. M. Blom, *Adv. Opt. Mater.* **2021**, *9*, 2101149.
- [32] B. van der Zee, Y. Li, G. A. H. Wetzelaer, P. W. M. Blom, *Adv. Electron. Mater.* **2022**, *8*, 2101261.
- [33] C. Féry, B. Racine, D. Vaufrey, H. Doyeux, S. Cinà, *Appl. Phys. Lett.* **2005**, *87*, 213502.
- [34] R. Meerheim, K. Walzer, M. Pfeiffer, K. Leo, *Appl. Phys. Lett.* **2006**, *89*, 061111.
- [35] S. Scholz, D. Kondakov, B. Luesem, K. Leo, *Chem. Rev.* **2015**, *115*, 8449.
- [36] C.-Y. Chan, M. Tanaka, Y.-T. Lee, Y.-W. Wong, H. Nakanotani, T. Hatakeyama, C. Adachi, *Nat. Photonics* **2021**, *15*, 203.
- [37] D. Karthik, Y. H. Jung, H. Lee, S. Hwang, B. Seo, J. Kim, C. W. Han, J. H. Kwon, *Adv. Mater.* **2021**, *33*, 2007724.
- [38] S. J. Yoon, J. H. Kim, W. J. Chung, J. Y. Lee, *Chem. – A Eur. J.* **2021**, *27*, 3065.
- [39] C. M. Hsieh, T. L. Wu, J. Jayakumar, Y. C. Wang, C. L. Ko, W. Y. Hung, T. C. Lin, H. H. Wu, K. H. Lin, C. H. Lin, S. Hsieh, C. H. Cheng, *ACS Appl. Mater. Interfaces* **2020**, *12*, 23199.
- [40] N. B. Kotadiya, A. Mondal, P. W. M. Blom, D. Andrienko, G. J. A. H. Wetzelaer, *Nat. Mater.* **2019**, *18*, 1182.
- [41] H. T. Nicolai, M. Kuik, G. A. H. Wetzelaer, B. De Boer, C. Campbell, C. Risko, J. L. Brédas, P. W. M. Blom, *Nat. Mater.* **2012**, *11*, 882.
- [42] H. T. Nicolai, M. M. Mandoc, P. W. M. Blom, *Phys. Rev. B* **2011**, *83*, 195204.
- [43] B. Van der Zee, Y. Li, G. A. H. Wetzelaer, P. W. M. Blom, *Adv. Mater.* **2022**, *34*, 2108887.
- [44] Y. Li, B. Van der Zee, G. A. H. Wetzelaer, P. W. M. Blom, *Adv. Electron. Mater.* **2021**, *7*, 2100155.
- [45] X. Zheng, R. Huang, C. Zhong, G. Xie, W. Ning, M. Huang, F. Ni, F. B. Dias, C. Yang, *Adv. Sci.* **2020**, *7*, 1902087.
- [46] L. Zhou, F. Ni, N. Li, K. Wang, G. Xie, C. Yang, *Angew. Chem., Int. Ed.* **2022**, *61*, e202203844.
- [47] N. Aizawa, Y. Pu, Y. Harabuchi, A. Nihonyanagi, R. Ibuka, H. Inuzuka, B. Dhara, Y. Koyama, K. Nakayama, S. Maeda, F. Araoka, D. Miyajima, *Nature* **2022**, *609*, 502.
- [48] T. A. Lin, T. Chatterjee, W. L. Tsai, W. K. Lee, M. J. Wu, M. Jiao, K. C. Pan, C. L. Yi, C. L. Chung, K. T. Wong, C. C. Wu, *Adv. Mater.* **2016**, *28*, 6976.